Chemical Science

ROYAL SOCIETY OF CHEMISTRY

EDGE ARTICLE

View Article Online
View Journal

Cite this: DOI: 10.1039/d6sc02393b

All publication charges for this article have been paid for by the Royal Society of Chemistry

Rationally designed tetrahedral-configuration-matching methane trap in a metal–organic framework for efficient CH_4/N_2 separation

Yating Wang,[a] Feifei Zhang,*[a] Yanan Yang,[a] Xiaoqing Wang,[a] Jinping Li *[ab] and Jiangfeng Yang *[a]

The enrichment and purification of CH_4 from coalbed methane by adsorption are important but challenging. We propose a "tetrahedral-configuration-matching" metal–organic framework (MOF) methane trap, TUTJ-3Ni, with cyclopropyl groups precisely positioned to create a pre-configured pore structure that is geometrically complementary to tetrahedral CH_4 molecules. TUTJ-3Ni exhibits a substantially higher CH_4 adsorption heat (30.3 kJ mol^{-1}) than its analogue TUTJ-2Ni (24.0 kJ mol^{-1}), and this value is the highest among reported adsorbents. Moreover, TUTJ-3Ni exhibits a superior CH_4/N_2 selectivity of 11.1, the highest value reported for hydrophobic MOFs. *In situ* spectroscopy and theoretical modeling results elucidate that the matched tetrahedral binding pocket, constructed with two hydrogen atoms of the cyclopropyl group along with fluorine and oxygen atoms from the ligand, engages all four hydrogen atoms of CH_4 *via* synergistic van der Waals interactions. Breakthrough experiment results verify that TUTJ-3Ni delivers high-purity CH_4 (>99.9%) from coalbed methane and that its dynamic CH_4 working capacity in humid environments is the highest among reported adsorbents. Furthermore, TUTJ-3Ni has good thermal and moisture stability and can easily be scaled up, making it promising for potential industrial applications.

Received 24th March 2026
Accepted 24th April 2026

DOI: 10.1039/d6sc02393b

rsc.li/chemical-science

1 Introduction

The global initiative to mitigate climate change and transition toward a low-carbon energy future has intensified the focus on unconventional natural gas resources. Among these, coalbed methane is a vast and promising reservoir.[1–3] However, the efficient utilization of a significant portion of coalbed methane, often termed low-concentration coalbed methane (methane content less than 50%),[4] remains a formidable challenge due to its inherently low calorific value. This gas stream is characterized by a high degree of dilution of methane (CH_4) with inert nitrogen (N_2).[5,6] The core scientific challenge lies in achieving thermodynamically favorable and kinetically efficient separation of CH_4 from N_2. These two molecules exhibit remarkably similar physical properties, including nearly identical kinetic diameters of 3.8 Å for CH_4 and 3.6 Å for N_2, coupled with low polarizabilities (Fig. S1 and Table S1).[7] This molecular similarity renders conventional separation technologies such as cryogenic distillation economically prohibitive.[8,9] Consequently, billions of cubic meters of this valuable energy resource are wasted annually, exacerbating global energy insecurity while unnecessarily contributing to greenhouse gas emissions.[10,11] The development of advanced separation materials capable of concurrently achieving high selectivity toward CH_4 and exceptional stability under practical operating conditions has therefore emerged as a critical technological frontier with profound global implications.

Metal–organic frameworks (MOFs), renowned for their ultrahigh surface areas and precisely tunable pore architectures, have emerged as promising candidates for gas separation.[12–32] Their chemical versatility allows researchers to design pore environments that are tailored for specific molecule recognition.[33,34] Researchers have made significant efforts to enhance the CH_4 affinity of porous materials. One common strategy is to incorporate polar functional groups (F, N, and O) as single-site ligands, *e.g.*, in fluorinated frameworks such as $CuIn(3\text{-}Fina)_4$,[35] nitrogen-containing structures such as $Ni(ina)_2$,[36] and oxygen-functionalized materials, including ATC-Cu.[37] The limited efficacy of these materials arises from two fundamental issues. First, their isolated sites interact with the tetrahedral CH_4 molecule *via* weak, non-specific van der Waals or electrostatic forces. Second, they fundamentally lack the complementary structural geometry required for specific molecular recognition. Consequently, they fail to provide a spatially matched and synergistic multi-point interaction that can enable the effective discrimination between CH_4 and N_2.

[a]College of Chemistry and Chemical Engineering, Taiyuan University of Technology, Taiyuan 030024, Shanxi Province, China. E-mail: zhangfeifei0096@link.tyut.edu.cn; jpli211@hotmail.com; yangjiangfeng@tyut.edu.cn

[b]Shanxi Research Institute of Huairou Laboratory, Taiyuan 030031, Shanxi Province, China

This limitation is particularly relevant given the presence of a substantial amount of water vapor in practical coalbed methane extraction. Under such humid conditions, competitive water adsorption severely diminishes the CH_4-adsorption performance. Water molecules readily form coordinate bonds with open metal sites or form extensive hydrogen-bonding networks, which in turn trigger irreversible structural collapse and pore blockage.[38,39] While recent efforts have focused on developing hydrophobic MOFs, often through perfluoroalkyl functionalization, these strategies raise concerns about environmental persistence and cost.[40,41] Overall, the establishment of a rational design principle that moves beyond mere hydrophobicity remains a formidable challenge. Such a principle must achieve specific, strong binding of the tetrahedral CH_4 molecule instead of the linear N_2, even in the presence of water.

Herein, we propose a "tetrahedral-configuration-matching" strategy inspired by the tetrahedral geometry of the methane molecule. As exhibited in Scheme 1, conventional adsorption sites—whether single, dual, or multiple—often suffer from insufficient binding strength or suboptimal spatial arrangement for effective CH_4 capture. Our design focuses on engineering adsorption sites that mimic and synergistically interact with the CH_4 tetrahedron. We focused on the methyl group ($-CH_3$) as an ideal functional moiety. Its intrinsic tetrahedral symmetry offers natural geometric complementarity to the CH_4 molecule, while the three outwardly directed hydrogen atoms increase the probability of optimal van der Waals contact. Furthermore, the well-established hydrophobicity of methyl groups ensures that performance is unaffected under moisture-rich conditions.[42,43] Therefore, we conducted an accurate molecule-level experiment to rigorously verify the effectiveness of this strategy and clarify the relationship between the structure and performance. We selected two pharmaceutical ligands (norfloxacin and ciprofloxacin), which are structurally identical except for a single variation: norfloxacin bears an ethyl group ($-CH_2CH_3$), while ciprofloxacin features a cyclopropyl group ($-CH_2CH_2-$). By incorporating these ligands into MOFs constructed from 4-*tert*-butylsulfonylcalix[4]arene ($H_4SC4A\text{-}SO_2$) and Ni(II) nodes, we synthesized two isostructural MOFs, denoted as TUTJ-2Ni (ethyl) and TUTJ-3Ni (cyclopropyl).

Our investigation reveals that TUTJ-3Ni (TUT = Taiyuan University of Technology; J = methane) exhibits exceptional CH_4 adsorption heat (30.3 kJ mol^{-1}), CH_4/N_2 selectivity (11.1), and water resistance, and it substantially outperforms TUTJ-2Ni. Through a combination of experimental characterization and theoretical calculations, we demonstrate that the cyclopropyl group is not merely a hydrophobic unit but a key structural element that enforces a pre-organized, rigid pore geometry. This geometry facilitates "tetrahedral configuration matching", enabling multi-point, synergistic dispersive interactions with the CH_4 molecule. Thus, in this study, a new paradigm is established for designing hydrophobic porous materials through geometry-guided molecular engineering for challenging energy- and environment-related separations, offering a new pathway to mitigate the trade-off between selectivity and hydrothermal stability.

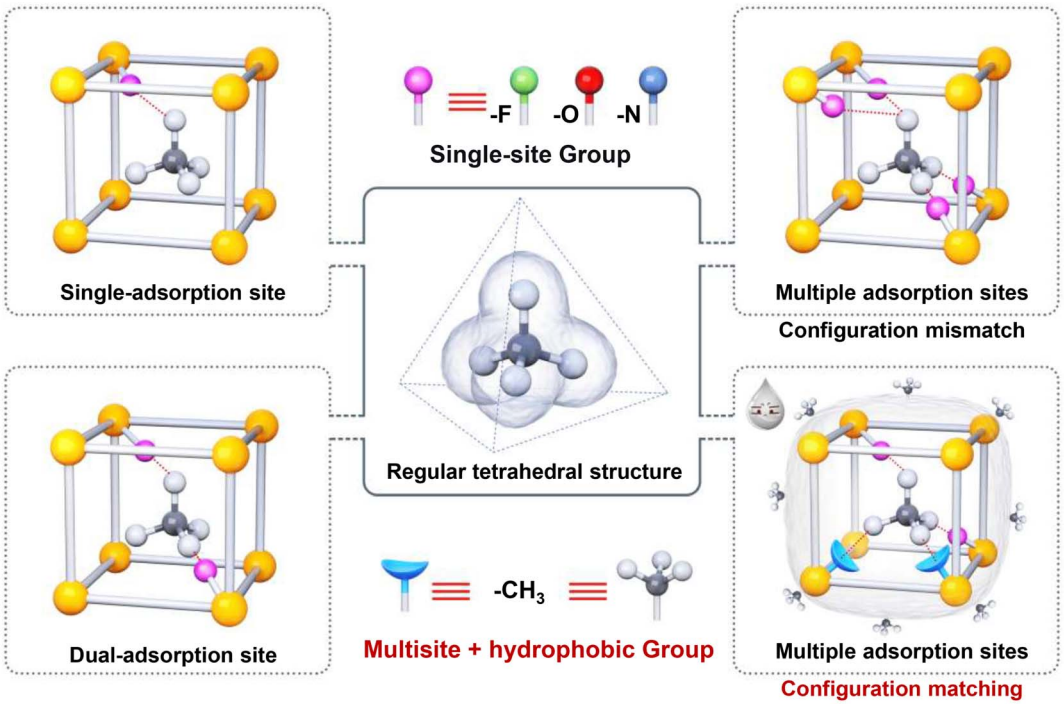

Scheme 1 The evolution of methane adsorption design from single/dual sites to configuration-mismatched multiple sites is presented, emphasizing the optimal strategy: combining tetrahedral-configuration-matching multiple adsorption sites with hydrophobic $-CH_3$ groups to achieve strong multi-point synergistic adsorption and excellent hydrophobicity. Green (–F), red (–O), dark blue (–N), and light blue ($-CH_3$).

2 Results and discussion

2.1 Structure and characterization

The MOFs TUTJ-2Ni and TUTJ-3Ni were synthesized under solvothermal conditions by using Ni(II) salts, $H_4SC4A\text{-}SO_2$, and norfloxacin or ciprofloxacin ligands, respectively. Experimental details are provided in the SI. The powder X-ray diffraction (PXRD) patterns of both MOFs showed excellent agreement with that of TUTJ-3Co, confirming their isostructural relationship (Fig. S2–S4). Accordingly, the crystal structures of TUTJ-2Ni and TUTJ-3Ni (Fig. S5–S8 and Table S2) were determined *via* Rietveld refinement using TUTJ-3Co as the initial structural model.[44]

As detailed in Fig. 1 and Table S2, structural analysis reveals that TUTJ-3Ni crystallizes in the monoclinic space group $P2_1/n$. Its fundamental secondary building unit consists of three Ni(II) ions, one $H_4SC4A\text{-}SO_2$ ligand, four ciprofloxacin molecules, and one nickel chloride hydrate unit. Two crystallographically equivalent Ni(II) centers exhibit identical coordination environments. Each Ni(II) ion forms coordinate bonds with sulfonyl and phenolic oxygen atoms from the $H_4SC4A\text{-}SO_2$ ligand, forming Ni–O bonds. In addition, they establish Ni–N and Ni–O bonds with nitrogen atoms and carboxylate oxygen atoms from two separate ciprofloxacin molecules. The third Ni(II) ion forms coordinate bonds with oxygen atoms of the calixarene skeleton and bridges two ciprofloxacin ligands *via* carboxylate oxygen atoms. The fourth Ni(II) center forms coordinate bonds with carboxylate oxygen atoms and carbonyl groups from two ciprofloxacin ligands, as well as with chloride ions and water molecules present in the starting materials.

These Secondary Building Units (SBUs) assemble into one-dimensional chains, wherein each calix[4]arene unit connects to four ciprofloxacin molecules. In the crystal lattice, these one-dimensional chains are not isolated. They undergo highly ordered parallel alignment along the other two crystallographic directions through interchain secondary π–π interactions, thereby assembling into a three-dimensional crystalline architecture.[42] The resulting structure features well-defined micropores with channel dimensions of approximately 12 × 6.5 $Å^2$ (Fig. S9 and S10). The structure of TUTJ-2Ni is similar to that of TUTJ-3Ni, differing only in the substitution of an ethyl moiety for the terminal cyclopropyl group in TUTJ-2Ni. This substitution results in a reduction of the channel dimensions from 12 × 7 $Å^2$ in TUTJ-2Ni to 12 × 6.5 $Å^2$ in TUTJ-3Ni. The narrowed pore size is expected to enhance host–guest compatibility. More importantly, the pre-organized cyclopropyl groups in TUTJ-3Ni create a geometrically optimized binding pocket that exhibits potential structural matching with the tetrahedral CH_4 molecule, whereas the ethyl groups in TUTJ-2Ni lead to a less defined pore architecture. Consequently, such precise geometric matching is expected to contribute to superior gas separation performance in the cyclopropyl-functionalized framework.

The phase purity of the as-synthesized TUTJ-2Ni and TUTJ-3Ni was confirmed by performing PXRD and SEM analyses. As shown in Fig. S11–S13, the experimental diffraction patterns of both materials exhibit excellent agreement with their respective simulated patterns, confirming successful synthesis with high crystallinity and phase purity. Thermogravimetric analysis (TGA) results reveal outstanding thermal stability for both frameworks (Fig. S14). TUTJ-2Ni maintained its structural integrity up to 573 K, while TUTJ-3Ni exhibited even enhanced stability, remaining stable up to 593 K. The TGA curves of the activated samples further corroborated these findings,

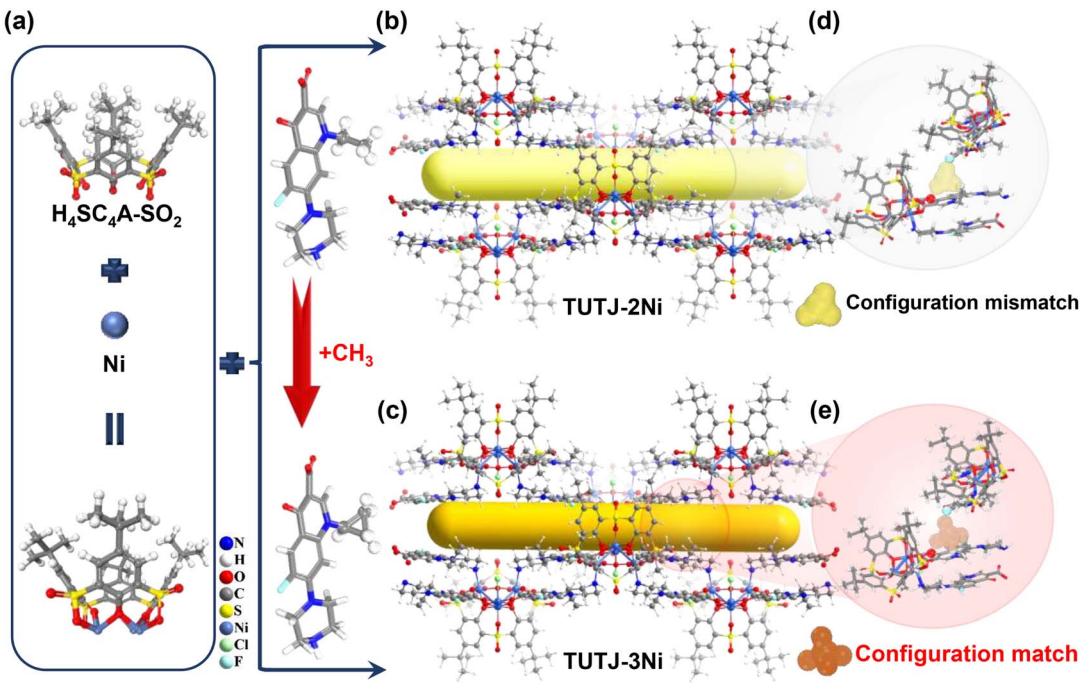

Fig. 1 Structure characterization of TUTJ-2Ni and TUTJ-3Ni. (a) Coordination environment of Ni(II) centers with the $H_4SC4A\text{-}SO_2$ ligand. (b and d) Structure of TUTJ-2Ni showing geometrically mismatched adsorption sites. (c and e) Structure of TUTJ-3Ni demonstrating geometrically matched tetrahedral binding pockets.

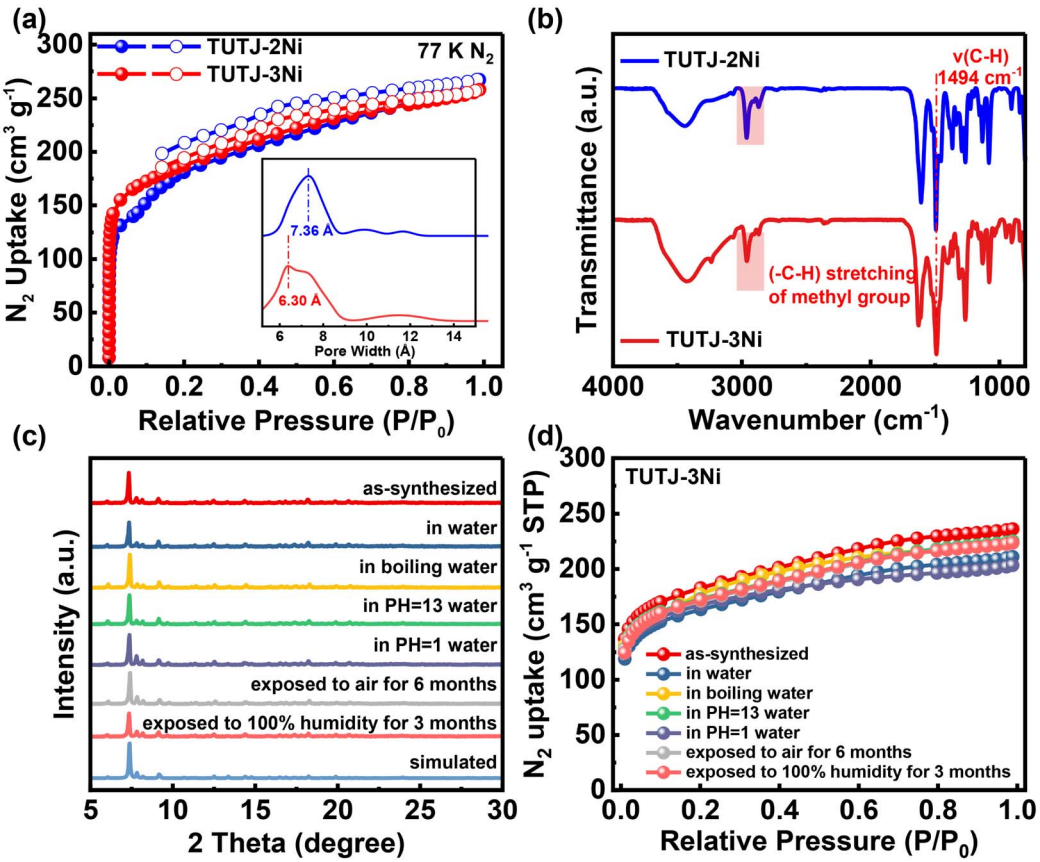

Fig. 2 Structural characterization and stability evaluation of TUTJ-2Ni and TUTJ-3Ni. (a) N_2 adsorption isotherms measured at 77 K and corresponding NLDFT pore size distributions (inset). (b) FT-IR spectra identifying characteristic functional groups in both frameworks. (c) PXRD patterns of TUTJ-3Ni after exposure to various extreme conditions (d) N_2 adsorption isotherms at 77 K of TUTJ-3Ni after treatment under different conditions.

indicating excellent thermal stability suitable for practical applications. The permanent porosity of activated TUTJ-2Ni and TUTJ-3Ni was confirmed by N_2 sorption measurements at 77 K (Fig. 2a and S15–S17). Both frameworks exhibit typical Type I isotherms, characteristic of microporous materials. The Brunauer–Emmett–Teller (BET) theory was used to determine the specific surface area that was found to be 614.5 $m^2\ g^{-1}$ for TUTJ-2Ni and 605.5 $m^2\ g^{-1}$ for TUTJ-3Ni, with corresponding total pore volumes of 0.41 $cm^3\ g^{-1}$ and 0.40 $cm^3\ g^{-1}$, respectively. Pore size distributions analyzed by the non-local density functional theory (NLDFT) revealed main peaks at 7.36 Å and 6.30 Å for TUTJ-2Ni and TUTJ-3Ni, respectively, demonstrating how the cyclopropyl substitution effectively reduces the pore dimensions while maintaining the structural integrity. Fourier-transform infrared (FT-IR) spectroscopy results enabled additional structural verification (Fig. 2b). Two sharp peaks observed at approximately 2965 cm^{-1} and 2867 cm^{-1} were attributed to C–H stretching vibrations of the $-CH_3$ groups, confirming the presence of abundant methyl groups in the framework.[45] Additional characteristic peaks at 1494 cm^{-1} were assigned to ν(C–H) vibrations, consistent with the expected chemical structure.

TUTJ-3Ni demonstrates exceptional stability under various extreme conditions, particularly maintaining complete structural integrity in highly humid environments. The framework remains unaffected after prolonged exposure to 100% relative humidity for a month, along with resistance to strong acids (pH = 1), bases (pH = 13), organic solvents, and high temperatures up to 573 K. The corresponding PXRD patterns and BET results (Fig. 2c, d and S18–S20) confirm the perfect preservation of the crystalline structure with no detectable degradation. This remarkable stability, especially the excellent water resistance, originates from the synergistic combination of several factors: (i) the rigid calix[4]arene scaffold that resists structural deformation; (ii) the fully coordinated Ni(II) centers with strong Ni–O and Ni–N bonds, which eliminate open metal sites prone to hydrolysis; (iii) the interdigitated chain architecture further stabilized by interchain π–π stacking interactions; and (iv) the hydrophobic pore surfaces decorated with abundant $-CH_3$ and cyclopropyl groups that effectively repel water molecules.[46] The outstanding moisture stability positions TUTJ-3Ni as an ideal candidate for practical separation applications under challenging humid conditions.

2.2 Gas adsorption performance

The gas adsorption performance of TUTJ-3Ni and TUTJ-2Ni was systematically investigated to evaluate their efficacy in

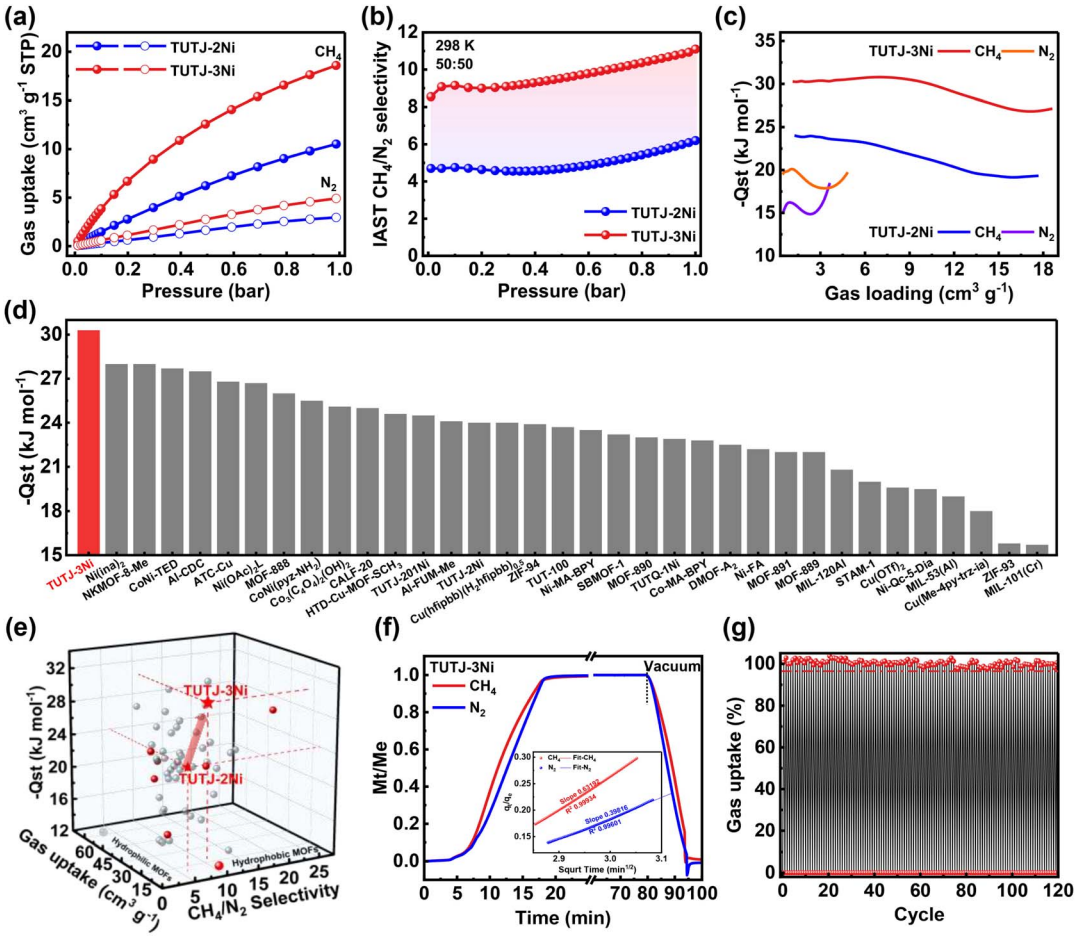

Fig. 3 Gas adsorption and separation performance. (a) CH_4 and N_2 sorption isotherms of TUTJ-2Ni and TUTJ-3Ni at 298 K. (b) IAST selectivity for a CH_4/N_2 (50 : 50) mixture of TUTJ-2Ni and TUTJ-3Ni at 298 K. (c) Q_{st} for CH_4 and N_2 on TUTJ-2Ni and TUTJ-3Ni. (d) Comparison of the CH_4 adsorption heat of TUTJ-3Ni with several representative benchmark adsorbents reported in the literature. (e) Three-dimensional performance comparison of TUTJ-3Ni with benchmark materials, correlating CH_4 uptake, selectivity, and Q_{st}. (f) Kinetic adsorption profiles of CH_4 and N_2 on TUTJ-3Ni at 298 K; the inset shows the corresponding diffusion time constants. (g) Cycling performance of TUTJ-3Ni over 120 adsorption–desorption cycles.

performing CH_4/N_2 separation. Single-component adsorption isotherms measured at 298 K demonstrate that TUTJ-3Ni achieves a CH_4 uptake of 18.6 $cm^3\ g^{-1}$ at 1 bar, substantially exceeding both its N_2 adsorption capacity (4.9 $cm^3\ g^{-1}$) and the CH_4 uptake of TUTJ-2Ni (10.5 $cm^3\ g^{-1}$), as shown in Fig. 3a and S21–S23. The pronounced difference in gas affinities between the two frameworks highlights the significant impact of ligand functionalization on the adsorption behavior.

The separation potential of these materials was further quantified through IAST selectivity calculations (Fig. 3b and S24). TUTJ-3Ni exhibits a CH_4/N_2 (50 : 50) selectivity of 11.1, markedly superior to the value of 6.19 observed for TUTJ-2Ni. This value represents the highest CH_4/N_2 selectivity among all compared hydrophobic MOFs (Table S4), including NKMOF-8-Me (9.0),[47] DMOF-A_2 (7.2),[48] TUT-100 (6.3),[49] and MIL-120Al (6.0),[50] positioning TUTJ-3Ni as the most effective material for CH_4/N_2 separation. Notably, IAST calculations for low-concentration CH_4/N_2 mixtures (20 : 80, 15 : 85 and 5 : 95) still give high selectivity, further supporting the practical applicability of TUTJ-3Ni for treating low-concentration coalbed methane.

Moreover, the heat of adsorption (Q_{st}), derived from adsorption isotherms collected at 273 and 298 K *via* the Clausius–Clapeyron equation, provides direct evidence of the enhanced CH_4 affinity of TUTJ-3Ni (Fig. S25–S27 and Table S3). The CH_4 adsorption heat of TUTJ-3Ni (30.3 kJ mol^{-1}) is significantly higher than that of TUTJ-2Ni (24.0 kJ mol^{-1}) (Fig. 3c). The CH_4 adsorption heat of TUTJ-3Ni was compared with those of several representative benchmark adsorbents, as summarized in Fig. 3d and Table S5. TUTJ-3Ni demonstrates the highest Q_{st} value among all the materials, such as $Ni(ina)_2$ (28.0 kJ mol^{-1}),[36] NKMOF-8-Me (28.0 kJ mol^{-1}),[47] CoNi-TED (27.7 kJ mol^{-1}),[51] and ATC-Cu (26.8 kJ mol^{-1}).[37] This comparison directly confirms the effectiveness of the "tetrahedral-geometry-matching" strategy, where the pre-organized cyclopropyl groups create a pore structure that maximizes van der Waals interactions with the tetrahedral CH_4 molecules.

A comprehensive three-dimensional performance assessment shows that TUTJ-3Ni is a promising CH_4/N_2 separation

material (Fig. 3e), as it demonstrates an optimal balance among adsorption capacity, selectivity, and binding strength. The exceptional performance of TUTJ-3Ni is attributed to the introduction of cyclopropyl groups, which generate geometrically matched adsorption sites exhibiting optimal complementarity to the tetrahedral CH_4 molecule—a feature absents in the ethyl-functionalized framework. The results of kinetic studies further demonstrate the separation capability of TUTJ-3Ni, which exhibits a kinetic selectivity of 1.59 for CH_4 over N_2, surpassing the value of 1.36 observed for TUTJ-2Ni (Fig. 3f and S28). Remarkably, complete desorption could be achieved within approximately 15 min under high vacuum conditions, indicating both favorable diffusion kinetics and excellent degree or regeneration of the material. From a practical perspective, TUTJ-3Ni demonstrates long-term stability, retaining over 97.5% of its initial CH_4 adsorption capacity at 1 bar and 298 K after 120 consecutive adsorption–desorption cycles under vacuum-assisted regeneration (Fig. 3g). This remarkable retention of performance, achieved through a simple and energy-efficient regeneration process, highlights the structural robustness of the framework and its strong potential for industrial separation applications requiring durable adsorbent materials. Therefore, TUTJ-3Ni is an advanced adsorbent material that combines configuration matching for selective CH_4 capture with rapid regeneration kinetics and long-term cycling stability, establishing a new standard for practical methane separation techniques.

2.3 Tetrahedral binding site identification

To elucidate the molecular-level mechanism underlying the superior CH_4/N_2 separation performance of TUTJ-3Ni, we employed a combination of *in situ* spectroscopic techniques and computational modeling. *In situ* infrared spectroscopy measurements were conducted to probe the host–guest interactions in both TUTJ-3Ni and TUTJ-2Ni frameworks (Fig. 4a–c, S29 and S30). As shown in Fig. 4a–c, upon CH_4 loading, two distinct vibrational bands emerge at 1303 and 3014 cm^{-1}, corresponding to δ(C–H) bending and ν(C–H) stretching modes, respectively.[52,53] The progressive intensification of these bands with increasing CH_4 exposure demonstrates the strong physical adsorption of methane within the framework, attributed to

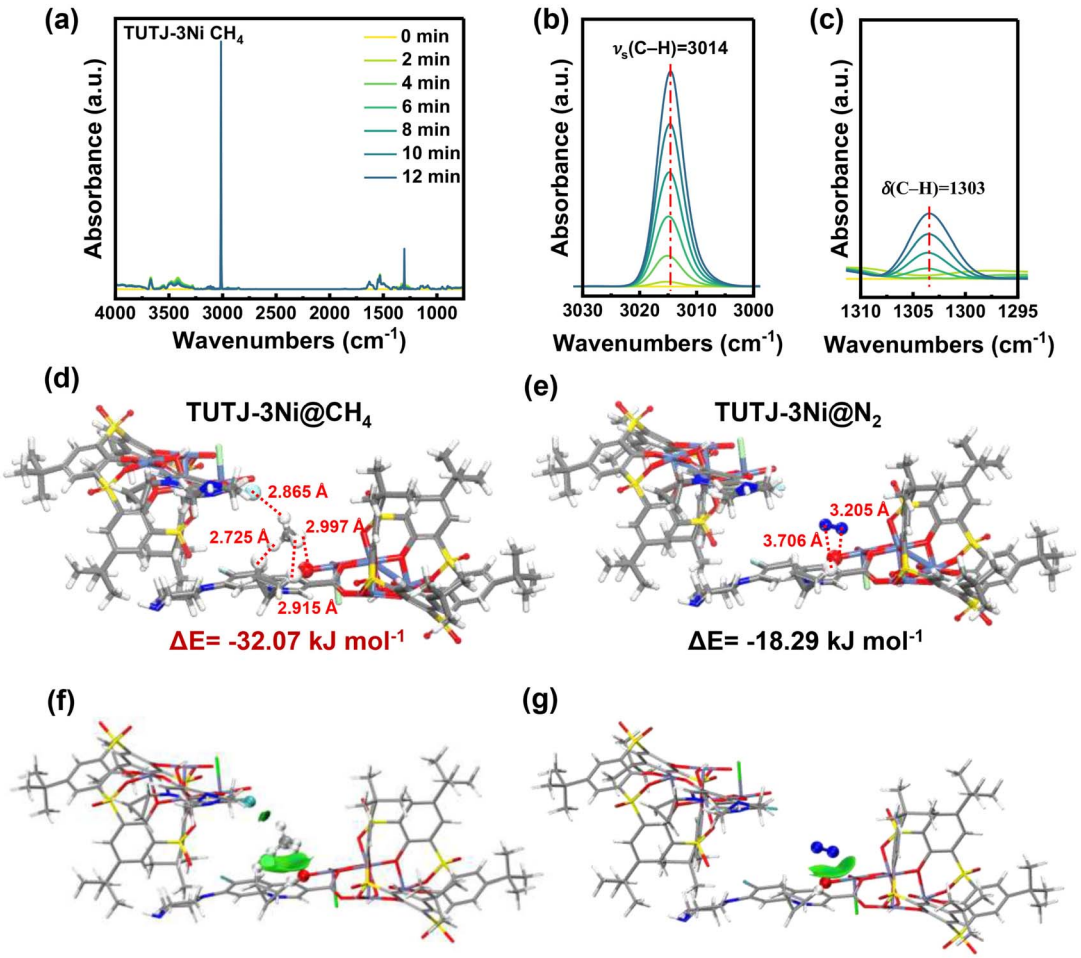

Fig. 4 Host–guest interactions and binding geometry in TUTJ-3Ni. (a) *In situ* FTIR spectra of CH_4-loaded TUTJ-3Ni. (b and c) Magnified views of characteristic regions from the *in situ* FTIR spectra. (d and e) DFT-optimized adsorption configurations of (d) CH_4 and (e) N_2 molecules within the pore structure. (f and g) Independent gradient model analysis based on Hirshfeld (IGMH) isosurfaces (isovalue = 0.002 a.u.) for (f) CH_4 and (g) N_2 on TUTJ-3Ni, where the green regions denote vdW-type interactions.

multiple van der Waals interactions between CH_4 molecules and the pore walls. In contrast, parallel measurements with N_2 revealed no discernible spectral features for either material (Fig. S30), confirming their weak affinity toward nitrogen. These spectroscopic results provide direct experimental evidence of the enhanced CH_4 adsorption capacity and selectivity in TUTJ-3Ni.

Theoretical modeling results provided molecular-level insight into the origin of the pronounced CH_4/N_2 separation performance of TUTJ-3Ni. Grand canonical Monte Carlo (GCMC) simulations at 298 K and 1 bar revealed that the adsorption density of CH_4 is significantly higher than that of N_2 within the framework, consistent with the experimental observations (Fig. S31). GCMC simulations initially identified three potential methane adsorption sites in TUTJ-3Ni. Analysis of site occupancy under reduced pressures showed that only two primary binding sites remain significantly populated at 0.1 bar. This finding allowed us to focus on the dominant adsorption site, which exhibits exceptional geometric complementarity to the tetrahedral CH_4 molecule (Fig. S32). The results of density functional theory (DFT) calculations on the optimized geometry provided atomic-level details of the host–guest interactions (Fig. 4d, e and S33–S35). The results demonstrated that all four hydrogen atoms of a single CH_4 molecule engage concurrently with various binding sites on the organic ligand. At this site, the CH_4 molecule establishes multiple specific contacts: C–H···F (2.865 Å) and C–H···O (2.999 Å) interactions exist, and notably, two C–H···H–C contacts are formed with the cyclopropyl group at distances of 2.725 Å and 2.915 Å (Fig. 4d). This achievement is in sharp contrast to other reported materials. Al-CDC provides only two binding sites, while TUTJ-201Ni offers three, both insufficient for optimal CH_4 engagement.[20,54] Although $Ni(ina)_2$ possesses four potential sites, their spatial arrangement permits interaction with merely three of the four hydrogen atoms of CH_4 owing to geometric mismatch.[36] In comparison, TUTJ-3Ni achieves complete tetrahedral coordination through its precisely aligned cyclopropyl functionalization. In stark contrast, the corresponding interactions in TUTJ-2Ni are substantially longer (C–H···F: 3.139 Å; C–H···O: 3.449 Å) and lack the defined geometric arrangement (Fig. S33). Furthermore, the calculated N_2 binding distances (3.205–3.706 Å) are substantially longer than the CH_4 binding distances (Fig. 4e), explaining the framework's pronounced selectivity toward methane capture through optimal geometric matching. As shown in Fig. S35, the binding energy calculated for the adsorption site I in TUTJ-3Ni reaches -32.07 kJ mol^{-1} for CH_4, which is substantially higher than that for N_2 (-18.29 kJ mol^{-1}) and significantly exceeds the CH_4 binding energy in the case of TUTJ-2Ni (-23.62 kJ mol^{-1}). These results align remarkably well with the experimentally derived values of the heat of adsorption, confirming the reliability of our theoretical models.

We performed an independent gradient model (IGM) analysis based on the DFT-optimized structures. The results visually demonstrate multiple van der Waals interactions between the hydrogen atoms of the CH_4 molecule and specific sites within the pore environment of TUTJ-3Ni. These interactions collectively establish a well-defined, tetrahedral-configuration-matching binding geometry that effectively encapsulates the CH_4 molecule (Fig. 4f). In contrast, such synergistic multi-point interaction patterns are notably absent in the case of N_2 adsorption on TUTJ-3Ni, and in both CH_4 and N_2 adsorption on TUTJ-2Ni (Fig. 4g and S36). TUTJ-2Ni cannot form a structurally complementary binding environment, and both frameworks exhibit inherently weak affinity toward the linear N_2 molecule. Collectively, the results of these multiscale investigations establish a direct correlation between the exceptional separation performance of TUTJ-3Ni and its structurally complementary adsorption geometry. The cyclopropyl-functionalized framework creates pre-organized binding pockets that enable optimized van der Waals interactions with tetrahedral CH_4 molecules, thus presenting a critical design principle for the development of advanced gas separation materials.

2.4 Dynamic breakthrough studies

We evaluated the industrial application potential of the developed materials for coalbed methane upgrading by performing dynamic breakthrough experiments using a custom-built apparatus (Fig. S37 and S38). When an equimolar CH_4/N_2 mixture at 5 mL min^{-1} was used, TUTJ-3Ni demonstrates exceptional separation efficacy, with N_2 eluting at 2.2 min g^{-1}, while CH_4 breaks through significantly later at 5.8 min g^{-1}, resulting in a substantial breakthrough time difference of 3.6 min g^{-1} (Fig. 5a). This pronounced retention contrast markedly surpasses the performance of TUTJ-2Ni, where both components break through at approximately 1.3 min g^{-1}, indicating inadequate separation capability. The practical versatility of TUTJ-3Ni was further validated through systematic evaluation across varying operational parameters. TUTJ-3Ni retains a robust separation performance under different flow conditions and CH_4/N_2 compositions (50 : 50, 20 : 80, 15 : 85, and 5 : 95), demonstrating its adaptability to fluctuating feed conditions commonly encountered in industrial settings (Fig. S39–S41). Notably, during He-purge desorption, high-purity CH_4 (>99.9%) can be efficiently recovered with negligible N_2 contamination (Fig. 5b), highlighting the material's renewability and potential for realizing pure-product collection. The framework exhibits outstanding cycling stability, maintaining identical breakthrough profiles over ten consecutive adsorption–desorption cycles (Fig. S42).

Because of the high-humidity environment that is characteristic of coalbed methane streams, we critically assessed the hydrophobicity and moisture stability of both materials. TUTJ-3Ni displays superior hydrophobicity with a water contact angle of 134° and minimal moisture uptake (Fig. S43). Most remarkably, the breakthrough performance of TUTJ-3Ni remains virtually unaffected under 100% relative humidity conditions (Fig. 5c), whereas TUTJ-2Ni suffers noticeable performance degradation (Fig. S44). This exceptional moisture tolerance is maintained over multiple cycles in saturated humidity environments, confirming the practical viability of TUTJ-3Ni for real-world methane purification applications (Fig. 5d). The comprehensive breakthrough studies establish TUTJ-3Ni as a technologically advanced adsorbent that

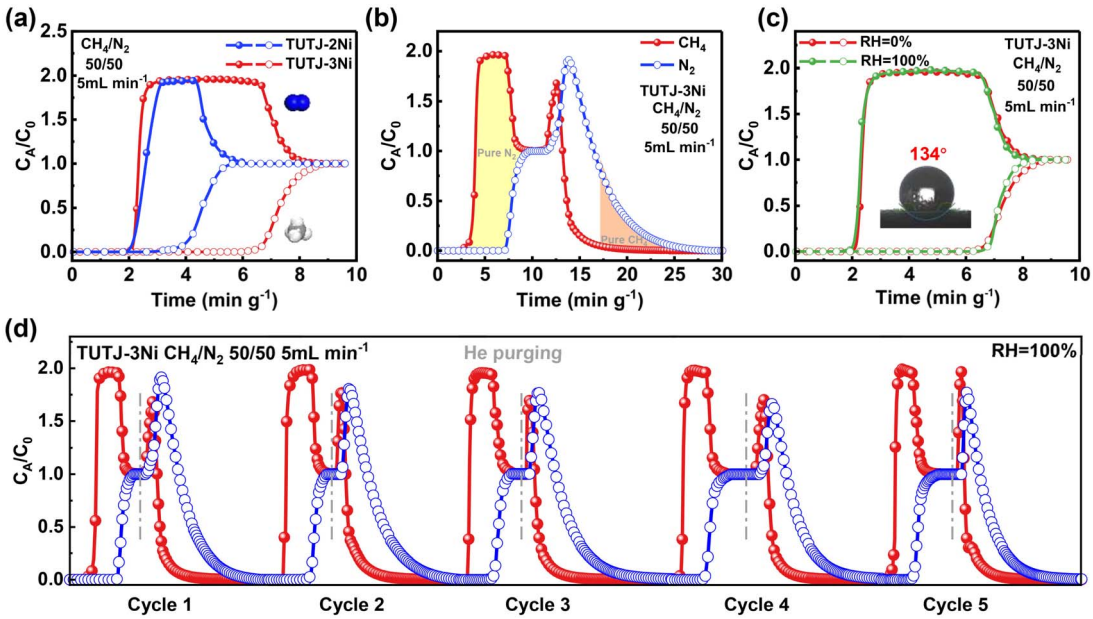

Fig. 5 Dynamic separation performance and stability evaluation. (a) Breakthrough curves for TUTJ-2Ni and TUTJ-3Ni with an equimolar CH_4/N_2 (50 : 50) mixture at 5 mL min^{-1}. (b) Adsorption–desorption breakthrough curves of TUTJ-3Ni for CH_4/N_2 (50 : 50) separation at 5 mL min^{-1}. (c) Comparison of breakthrough curves under dry (RH = 0%) and humid (RH = 100%) conditions for CH_4/N_2 (50 : 50) at 5 mL min^{-1}; the inset shows the water contact angle of TUTJ-3Ni. (d) Cycling breakthrough performance of TUTJ-3Ni over five consecutive adsorption–desorption cycles under humid (RH = 100%) CH_4/N_2 (50 : 50) flow at 5 mL min^{-1}. For comparison, the *x* axis is normalized to "time per gram of adsorbents".

combines CH_4 affinity with exceptional hydrolytic stability, enabling efficient methane recovery from nitrogen-diluted streams under relevant practical-operation conditions. The material demonstrates robust performance with varying feed compositions, excellent regeneration, and sustained efficiency in humid environments. These qualities position it as a promising candidate for industrial coalbed methane upgrading.

2.5 Hydrolytic stability and practical performance validation

The practical applicability of TUTJ-3Ni under humid conditions was assessed through comparative studies with three benchmark CH_4/N_2 separation materials: ATC-Cu,[37] $Ni(ina)_2$,[36] and CoNi-TED.[51] Contact angle measurements revealed that TUTJ-3Ni exhibits exceptional hydrophobicity (134°), while water droplets were instantly absorbed by the benchmark materials (Fig. S45 and S46). After one week of aging at 100% relative humidity, TUTJ-3Ni retained its crystalline structure, whereas ATC-Cu and CoNi-TED showed significant peak attenuation, and $Ni(ina)_2$ underwent complete structural collapse (Fig. S47). Correspondingly, TUTJ-3Ni retained over 93% of its original CH_4 and N_2 uptake capacity, while the reference materials suffered substantial capacity loss (Fig. S48–S52). Under dry feed conditions, all four materials demonstrated effective CH_4/N_2 separation (Fig. S53). However, upon exposure to 100% relative humidity, the benchmark materials exhibited progressive performance degradation with each cycle, while TUTJ-3Ni retained consistent separation efficiency over five consecutive cycles (Fig. S54–S58). Quantitative analysis showed that TUTJ-3Ni achieved the highest CH_4 working capacity under dry conditions (18.27 $cm^3\ g^{-1}$) and retained 98% of this capacity after five humid cycles, compared to only 5–42% retention for the reference materials (Fig. S59–S61). Radar chart analysis (Fig. S62) integrating breakthrough time, adsorption capacity, and dynamic performance metrics confirmed that TUTJ-3Ni retained >93% of all evaluated parameters under harsh humid conditions, significantly outperforming the benchmark materials (5–80%) and establishing it as a leading candidate for practical coalbed methane upgrading.

The transition from laboratory-scale synthesis to industrial implementation represents a critical step in MOF development. To identify the scalability challenges, we successfully synthesized a TUTJ-3Ni sample with a 100-fold increase in scale while maintaining excellent phase purity (Fig. S63), as confirmed by PXRD analysis results (Fig. S64a). The scaled-up and laboratory-scale specimens exhibit nearly identical gas adsorption capacity and selectivity (Fig. S64b), demonstrating the viability of large-scale production without compromising performance. This successful scale-up, combined with the exceptional hydrolytic stability and separation performance, positions TUTJ-3Ni as a technologically advanced adsorbent ready for industrial applications in coalbed methane purification.

3 Conclusions

In summary, we have successfully demonstrated a geometry-guided molecular engineering strategy for overcoming the ubiquitous trade-off between selectivity and hydrothermal stability in CH_4/N_2 separation. By incorporating rigid cyclopropyl groups into the framework of TUTJ-3Ni, we constructed a pre-organized pore environment with exceptional geometric

complementarity to the tetrahedral CH_4 molecule, which enables synergistic multi-point van der Waals interactions for highly selective methane capture. This "tetrahedral-configuration-matching" strategy endows TUTJ-3Ni with remarkable CH_4/N_2 selectivity, and, most importantly, excellent hydrolytic stability, maintaining its structural integrity and separation performance even under 100% relative humidity. The material's practical viability is unequivocally confirmed by its excellent dynamic separation efficiency, robust cyclability, and successful scale-up. Therefore, this work establishes a new paradigm for designing hydrophobic adsorbents *via* geometric matching. It offers a promising path for advanced energy-related separations under challenging practical conditions.

Author contributions

Y. W. and F. Z. conceived and designed the research. Y. W. and Y. Y. performed most of the experiments. X. W. and F. Z. analysed the data. Y. W. and F. Z. wrote the manuscript. J. L. and J. Y. supervised the project. All authors participated in and contributed to the preparation of the manuscript.

Conflicts of interest

There are no conflicts to declare.

Data availability

CCDC 2492179 (for TUTJ-2Ni), 2492185 (for TUTJ-3Ni) and 2495218 (for TUTJ-3Co) contain the supplementary crystallographic data for this paper.[44a–c]

The data that support the findings of this study are openly available in the supplementary information (SI). Supplementary information: experimental procedures, gas adsorption isotherms, crystallographic data, and theoretical computational details. See DOI: https://doi.org/10.1039/d6sc02393b.

Acknowledgements

This work was financially supported by the National Natural Science Foundation of China (No. 22408258, 22478272, and 22378287), Joint Funds of the National Natural Science Foundation of China (U25A20624) and Natural Science Foundation of Shanxi Province (No. 202303021222012).

Notes and references

1 L. Grant, I. Vanderkelen, L. Gudmundsson, E. Fischer, S. I. Seneviratne and W. Thiery, Global emergence of unprecedented lifetime exposure to climate extremes, *Nature*, 2025, **641**, 374–379.
2 J. C. Stroeve, D. Notz, J. Dawson, E. A. G. Schuur, D. Dahl-Jensen and C. Giesse, Disappearing landscapes: The Arctic at +2.7°C global warming, *Science*, 2025, **387**, 616–621.
3 E. McFarland, Unconventional Chemistry for Unconventional Natural Gas, *Science*, 2012, **338**, 340–342.
4 C. Liu, Y. Zhou, Y. Sun, W. Su and L. Zhou, Enrichment of coal-bed methane by PSA complemented with CO_2 displacement, *AIChE J.*, 2011, **57**, 645–654.
5 H. Shang, F. Zhang, J. Liu, X. Zhang, J. Yang, L. Li and J. Li, Enriching Low-Concentration Coalbed Methane Using a Hydrophobic Adsorbent under Humid Conditions, *Ind. Eng. Chem. Res.*, 2021, **60**, 12689–12697.
6 T. A. Moore, Coalbed methane: A review, *Int. J. Coal Geol.*, 2012, **101**, 36–81.
7 L. Li, L. Yang, J. Wang, Z. Zhang, Q. Yang, Y. Yang, Q. Ren and Z. Bao, Highly efficient separation of methane from nitrogen on a squarate-based metal-organic framework, *AIChE J.*, 2018, **64**, 3681–3689.
8 D. M. Ruthven, Past Progress and Future Challenges in Adsorption Research, *Ind. Eng. Chem. Res.*, 2000, **39**, 2127–2131.
9 Y. Gensterblum, A. Busch and B. M. Krooss, Molecular concept and experimental evidence of competitive adsorption of H_2O, CO_2 and CH_4 on organic material, *Fuel*, 2014, **115**, 581–588.
10 D. S. Sholl and R. P. Lively, Seven chemical separations to change the world, *Nature*, 2016, **532**, 435–437.
11 S. J. Davis and C. Shearer, A crack in the natural-gas bridge, *Nature*, 2014, **514**, 436–437.
12 X. Han, H. G. W. Godfrey, L. Briggs, A. J. Davies, Y. Cheng, L. L. Daemen, A. M. Sheveleva, F. Tuna, E. J. L. McInnes, J. Sun, C. Drathen, M. W. George, A. J. Ramirez-Cuesta, K. M. Thomas, S. Yang and M. Schröder, Reversible adsorption of nitrogen dioxide within a robust porous metal–organic framework, *Nat. Mater.*, 2018, **17**, 691–696.
13 S. Zhou, O. Shekhah, A. Ramírez, P. Lyu, E. Abou-Hamad, J. Jia, J. Li, P. M. Bhatt, Z. Huang, H. Jiang, T. Jin, G. Maurin, J. Gascon and M. Eddaoudi, Asymmetric pore windows in MOF membranes for natural gas valorization, *Nature*, 2022, **606**, 706–712.
14 M. Eddaoudi, J. Kim, N. Rosi, D. Vodak, J. Wachter, M. O'Keeffe and O. M. Yaghi, Systematic Design of Pore Size and Functionality in Isoreticular MOFs and Their Application in Methane Storage, *Science*, 2002, **295**, 469–472.
15 J.-R. Li, R. J. Kuppler and H.-C. Zhou, Selective gas adsorption and separation in metal–organic frameworks, *Chem. Soc. Rev.*, 2009, **38**, 1477–1504.
16 H.-C. Zhou, J. R. Long and O. M. Yaghi, Introduction to Metal–Organic Frameworks, *Chem. Rev.*, 2012, **112**, 673–674.
17 H. Furukawa, K. E. Cordova, M. O'Keeffe and O. M. Yaghi, The Chemistry and Applications of Metal-Organic Frameworks, *Science*, 2013, **341**, 1230444.
18 F. Zhang, Z. Zhao, Y. Wang, X. Li, X. Bai, M. Lu, Y. Wang, X. Wang, L. Li, J. Li and J. Yang, Nitrogen Adsorption Sites with Low Polarizability for Benchmark N_2/CH_4 Separation, *Angew. Chem., Int. Ed.*, 2025, **64**, e202510242.
19 H. Zhang, J. Tang, C. Yu, M. Zhang, J. Wang and J. Duan, Oriented design and engineering of advanced metal–organic frameworks for light hydrocarbon separations, *Chem. Sci.*, 2025, **16**, 11768–11800.
20 Z. Zhu, J. Xiao, M. Zhang, Y. Huang and S. Yuan, Precision pore engineering via fit-topology assembly in a Zn-

porphyrin MOF for selective C_2H_2 capture, *Chem. Sci.*, 2025, **16**, 22638–22646.
21 H. Li, M. Eddaoudi, M. O'Keeffe and O. M. Yaghi, Design and synthesis of an exceptionally stable and highly porous metal-organic framework, *Nature*, 1999, **402**, 276–279.
22 S. Kitagawa, R. Kitaura and S.-i. Noro, Functional Porous Coordination Polymers, *Angew. Chem., Int. Ed.*, 2004, **43**, 2334–2375.
23 P. Li, N. A. Vermeulen, C. D. Malliakas, D. A. Gómez-Gualdrón, A. J. Howarth, B. L. Mehdi, A. Dohnalkova, N. D. Browning, M. O'Keeffe and O. K. Farha, Bottom-up construction of a superstructure in a porous uranium-organic crystal, *Science*, 2017, **356**, 624–627.
24 R.-B. Lin, Z. Zhang and B. Chen, Achieving High Performance Metal–Organic Framework Materials through Pore Engineering, *Acc. Chem. Res.*, 2021, **54**, 3362–3376.
25 F. Zhang, H. Shang, L. Wang, Y. Wang, J. Yang, Y. Xia, H. Li, L. Li and J. Li, Construction of a Porous Metal–Organic Framework with a High Density of Open Cr Sites for Record N_2/O_2 Separation, *Adv. Mater.*, 2021, **33**, 2100866.
26 F. Zhang, H. Shang, B. Zhai, Z. Zhao, Y. Wang, L. Li, J. Li and J. Yang, Synergistic Nitrogen Binding Sites in a Metal-Organic Framework for Efficient N_2/O_2 Separation, *Angew. Chem., Int. Ed.*, 2023, **62**, e202316149.
27 Y.-L. Zhao, X. Bai, X. Zhang, Z.-Y. Han and J.-R. Li, Record high CH_4/N_2 adsorption separation selectivity in a scalable metal-organic framework, *Sci. Bull.*, 2025, **70**, 1215–1218.
28 R.-B. Lin, S. Xiang, W. Zhou and B. Chen, Microporous Metal-Organic Framework Materials for Gas Separation, *Chem*, 2020, **6**, 337–363.
29 K. M. Carsch, H. Z. H. Jiang, R. A. Klein, A. S. Rosen, P. S. Summerhill, J. L. Peltier, A. J. Huang, R. A. Murphy, M. N. Dods, H. A. Silva, Z. Hasanbasri, H. Kwon, S. L. Karstens, Y. Yabuuchi, J. Börgel, J. W. Taylor, K. R. Meihaus, K. C. Bustillo, A. M. Minor, K. A. Persson, C. M. Brown, R. D. Britt, N. P. Stadie and J. R. Long, Multigas adsorption with single-site cooperativity in a metal–organic framework, *Science*, 2025, **390**, 808–812.
30 O. I.-F. Chen, C.-H. Liu, K. Wang, E. Borrego-Marin, H. Li, A. H. Alawadhi, J. A. R. Navarro and O. M. Yaghi, Water-Enhanced Direct Air Capture of Carbon Dioxide in Metal–Organic Frameworks, *J. Am. Chem. Soc.*, 2024, **146**, 2835–2844.
31 Z. Chen, K. O. Kirlikovali, P. Li and O. K. Farha, Reticular Chemistry for Highly Porous Metal–Organic Frameworks: The Chemistry and Applications, *Acc. Chem. Res.*, 2022, **55**, 579–591.
32 Z.-M. Ye, Y. Xie, K. O. Kirlikovali, S. Xiang, O. K. Farha and B. Chen, Architecting Metal–Organic Frameworks at Molecular Level toward Direct Air Capture, *J. Am. Chem. Soc.*, 2025, **147**, 5495–5514.
33 A. Schneemann, V. Bon, I. Schwedler, I. Senkovska, S. Kaskel and R. A. Fischer, Flexible metal–organic frameworks, *Chem. Soc. Rev.*, 2014, **43**, 6062–6096.
34 G. Armstrong, Marvellous MOFs, *Nat. Chem.*, 2008, DOI: 10.1038/nchem.41.
35 L.-P. Zhang, L. Xu, X.-T. Zhang, Y.-T. Li, H.-L. Lan, S.-C. Liu and Q.-Y. Yang, Pore Chemical Modification of Bimetallic Coordination Networks for Coal-Bed Methane Purification under Humid Conditions, *Inorg. Chem.*, 2025, **64**, 1596–1603.
36 S.-M. Wang, M. Shivanna and Q.-Y. Yang, Nickel-Based Metal–Organic Frameworks for Coal-Bed Methane Purification with Record CH_4/N_2 Selectivity, *Angew. Chem., Int. Ed.*, 2022, **61**, e202201017.
37 Z. Niu, X. Cui, T. Pham, P. C. Lan, H. Xing, K. A. Forrest, L. Wojtas, B. Space and S. Ma, A Metal–Organic Framework Based Methane Nano-trap for the Capture of Coal-Mine Methane, *Angew. Chem., Int. Ed.*, 2019, **131**, 10244–10247.
38 J. J. Low, A. I. Benin, P. Jakubczak, J. F. Abrahamian, S. A. Faheem and R. R. Willis, Virtual High Throughput Screening Confirmed Experimentally: Porous Coordination Polymer Hydration, *J. Am. Chem. Soc.*, 2009, **131**, 15834–15842.
39 T. He, X.-J. Kong and J.-R. Li, Chemically Stable Metal–Organic Frameworks: Rational Construction and Application Expansion, *Acc. Chem. Res.*, 2021, **54**, 3083–3094.
40 S. Pal, S. Kulandaivel, Y.-C. Yeh and C.-H. Lin, Recent trends in superhydrophobic metal–organic frameworks and their diverse applications, *Coord. Chem. Rev.*, 2024, **518**, 216108.
41 M. Zheng, W. Xue, T. Yan, Z. Jiang, Z. Fang, H. Huang and C. Zhong, Fluorinated MOF-Based Hexafluoropropylene Nanotrap for Highly Efficient Purification of Octafluoropropane Electronic Specialty Gas, *Angew. Chem., Int. Ed.*, 2024, **63**, e202401770.
42 F. Zhang, Z. Zhao, Y. Wang, Y. Tang, X. Li, X. Bai, M. Lu, L. Li, J. Li and J. Yang, Installing Methyl Group Guards in a Metal–Organic Framework Featuring Multiple N/O Active Sites for Efficient C_2H_2/CO_2 Separation under Moist Conditions, *ACS Mater. Lett.*, 2024, **6**, 4482–4490.
43 T. Li, L. Zhang, Y. Wang, X. Jia, H. Chen, Y. Li, Q. Shi, L.-B. Sun, J. Li, B. Chen and L. Li, Optimizing supramolecular interactions within metal–organic frameworks for ultra-high purity propylene purification, *AIChE J.*, 2025, **71**, e18646.
44 (*a*) CCDC 2492179: Experimental Crystal Structure Determination, 2026, DOI: 10.5517/ccdc.csd.cc2pn9wk; (*b*) CCDC 2492185: Experimental Crystal Structure Determination, 2026, DOI: 10.5517/ccdc.csd.cc2pnb2s; (*c*) CCDC 2495218: Experimental Crystal Structure Determination, 2026, DOI: 10.5517/ccdc.csd.cc2prgxv.
45 Z. Zhao, Y. Li, Y. Wang, Y. Wang, Y. Tang, M. Lu, X. Yang, X. Wang, F. Zhang, J. Li and J. Yang, Hydrophobic metal-organic framework Featuring multiple O/S active sites for efficient CH4/N2 separation under humid conditions, *Sep. Purif. Technol.*, 2025, **361**, 131382.
46 I. V. Khariushin, V. Bulach, S. E. Solovieva, I. S. Antipin, A. S. Ovsyannikov and S. Ferlay, Thiacalix[4]arene macrocycles as versatile building blocks for the rational design of high-nuclearity metallic clusters, metallamacrocycles, porous coordination cages and containers, *Coord. Chem. Rev.*, 2024, **513**, 215846.

47 M. Chang, F. Wang, Y. Wei, Q. Yang, J.-X. Wang, D. Liu and J.-F. Chen, Separation of CH4/N2 by an ultra-stable metal–organic framework with the highest breakthrough selectivity, *AIChE J.*, 2022, **68**, e17794.

48 T. Li, X. Jia, H. Chen, Z. Chang, L. Li, Y. Wang and J. Li, Tuning the Pore Environment of MOFs toward Efficient CH_4/N_2 Separation under Humid Conditions, *ACS Appl. Mater. Interfaces*, 2022, **14**, 15830–15839.

49 J. Liu, X. Tang, X. Liang, L. Wu, F. Zhang, Q. Shi, J. Yang, J. Dong and J. Li, Superhydrophobic zeolitic imidazolate framework with suitable SOD cage for effective CH_4/N_2 adsorptive separation in humid environments, *AIChE J.*, 2022, **68**, e17589.

50 F. Zhang, H. Shang, B. Zhai, X. Li, Y. Zhang, X. Wang, J. Li and J. Yang, Thermodynamic-kinetic synergistic separation of CH_4/N_2 on a robust aluminum-based metal-organic framework, *AIChE J.*, 2023, **69**, e18079.

51 P. Guo, J. Fu, B. Xue, T. Wang, L. Yang, Y. Ying, Q. Yang and D. Liu, One Flexible Metal–Organic Framework with Guest-Adaptive Rotational Valve for Gas Separation, *Adv. Funct. Mater.*, 2025, **35**, 2500210.

52 P. Liu, L. Fan, J. Li, Z. Wu, Y. Wang, Y. Chen, J. Gao, J. Yang, J. Li, B. Chen and L. Li, A Microporous Titanium Metal–Organic Framework with Double Nanotraps for Record CH_4/N_2 Separation, *Chem. Mater.*, 2024, **36**, 2925–2932.

53 M. Chang, Y. Li, M. Tong, J. Yang, T. Ma, Y. Wang and J. Zheng, Synergistic Binding Sites in a Robust and Scalable Metal–Organic Framework for Record CH_4 Capture, *Small*, 2025, **21**, 2412121.

54 M. Chang, Y. Zhao, D. Liu, J. Yang, J. Li and C. Zhong, Methane-trapping metal–organic frameworks with an aliphatic ligand for efficient CH_4/N_2 separation, *Sustainable Energy Fuels*, 2020, **4**, 138–142.